*Materials Research.* 2019; 22(5): e20190230
DOI: http://dx.doi.org/10.1590/1980-5373-MR-2019-0230

# Austenitic Grain Size Prediction in Hot Forging of a 20mncr5 Steel by Numerical Simulation Using the JMAK Model for Industrial Applications

***Thiago Marques Ivaniski*[a]*, Jérémy Epp[b], Hans-Werner Zoch[b], Alexandre da Silva Rocha[a]**

[a]*Laboratório de Transformação Mecânica (LdTM), Universidade Federal do Rio Grande do Sul (UFRGS), Porto Alegre, RS, Brasil*
[b]*Leibniz-Institut für Werkstofforientierte Technologien (IWT), Bremen, Germany*

Received: March 11, 2019; Revised: September 26, 2019; Accepted: October 2, 2019

Yield strength and toughness in steels are directly associated with hot forging processes, especially by controlling austenitic grain size and cooling conditions. The phenomenological JMAK model in macroscale has been applied in different material classes to predict grain size after hot forming. However, on an industrial application, there is still a lack of understanding concerning the synergic effects of strain rate and temperature on recrystallization. This preliminary study aimed at investigating the applicability of coupled semi-empirical JMAK and visco-elastoplastic models in numerical simulation to predict austenitic grain size (PAGS). Hot forging of cylindrical samples of a ferritic-perlitic DIN 20MnCr5 steel was performed followed by water quenching. The main influences, such as temperature, strain and strain rate fields following the recrystallization model were investigated using the subroutine of FORGE NxT 2.1 software. The results were evaluated by comparing experimentally measured and simulated PAGS at process end. The forging process generates different strain and strain rate fields in the workpiece, which in turn lead to a variation in the PAGS and recrystallization fractions. The simulation was able to detect the PAGS variation showing a good agreement between the experimental forging results and the applied model.

**Keywords:** *Numerical simulation, JMAK's model, hot forging, grain size*

## 1. Introduction

Microstructure control is a key to the development of high-performance alloy steels, especially for applications requiring toughness, high fatigue strength and hardness in automotive components. Several studies report the phenomena of hardening, dynamic recovery, dynamic recrystallization and austenitic grain growth, and how these phenomena affect the steel mechanical properties. The control of such mechanisms by thermomechanical processing is most commonly implemented in rolling processes[1-6]. However, they are often more challenging to be implemented for forging processes. As an economically feasible alternative that has excellent potential for forging solutions, Finite Element Method (FEM) using computer simulation seeks to reduce the try-outs in an industrial scenario.

Moreover, the classic JMAK model (Johnson-Mehl-Avrami-Kolmogorov) is mathematically stable and can be applied to predict recrystallization and grain growth phenomena[7]. The JMAK model is presently available in several numerical simulation software. For more than a decade it has been shown that the semi-empirical analytical model JMAK can describe the global recrystallization kinetics (Eq. 1), where $X(t)$ represents the recrystallized grain fraction as a function of time ($t$).

$$X(t) = 1 - e^{-b.t^n} \quad (1)$$

The exponent ($b$) represents the Avrami coefficient, therefore very sensitive to variation in temperature. The Avrami exponent ($n$) is related to the mechanism of phase transformation, for example, if the nucleation rate remains constant or even increases during the transformation progress or if the nucleation rate reaches zero soon after the onset of growth.

Many articles report the strong influence of parameters such as temperature, deformation and strain rate on dynamic ($X_{DRX}$), metadynamic ($M_{DRX}$) and static ($S_{RX}$) recrystallization[8-10]. Innovative studies have considered the quantitative dependence of $X_{DRX}$ activation energy and strain rate exponent on the temperature variation in high carbon steels. They also were successful in minimizing errors between the experimental values and correspondent finite element solutions using optimization tools[11-13]. However, there are some implications concerning the validation of a robust model for hot forging processes that should be considered, such as thermomechanical history, complex strain fields, fibering zones as well as steady-state conditions in flow curves. These influences are not isolated in forged parts and are driven by industrial demands. Therefore, more efforts must be given to reach more accurate results by FEM simulation models in industrial forging applications.

This preliminary study aimed at investigating the applicability of a semi-empirical model of JMAK coupled to the visco-elastoplastic model in numerical simulation.

*e-mail: thiago.ivaniski@ufrgs.br

A ferritic-perlitic DIN 20MnCr5 steel microstructural was used to carry out this work. Subsequent steps of the process were performed to represent an industrial process. The main influences, such as temperature, strain and strain rate fields following the recrystallization model were investigated using a subroutine of the FORGE NxT 2.1 software.

## 2. Materials and Methods

### *2.1 Acquiring the experimental data*

Cylindrical samples with a diameter of 25.4 mm and a height of 35 mm were manufactured from a DIN 20MnCr5 steel. The chemical composition of the steel is shown in Table 1. Hot forging (upsetting) experiments were carried out in a hydraulic press with a capacity of 400 kN, as shown schematically in Figure 1. Samples were heated in the furnace to 1200 ºC and then moved to the press where a 60% reduction in height was applied. The temperature evolution in the workpiece was measured by a thermal imager Fluke® Ti400. The temperature frames obtained by the thermal imager were corrected by thermocouple analysis for higher accuracy in the temperature determination. After that, the collected results were used as boundary conditions into the Forge® software. The austenitic grain size was analysed by Optical Microscopy following the ASTM E112 standard. The forged samples were quenched in water directly after forging to stop changes in grain size, in order to preserve the austenitic grain size from deformation end. Samples were etched to reveal the prior austenite grain boundaries (PAGBs) with an etching prepared with 3g of picric acid in a solution of 30% liquid detergent in water.

**Table 1.** Chemical composition of the experimental DIN 20MnCr5.

| % wt | C | Si | Mn | Cr |
|---|---|---|---|---|
| | 0.19 | 0.2 | 1.25 | 1.15 |

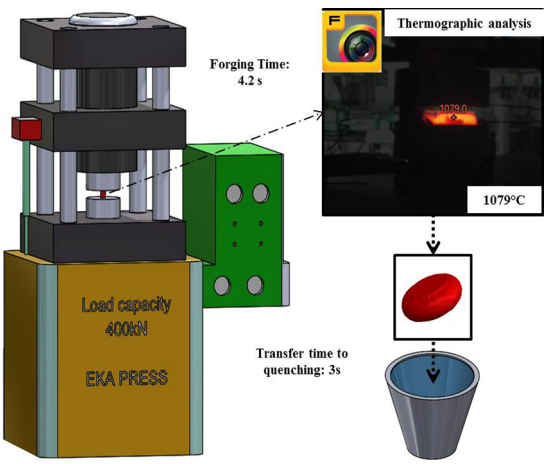


**Figure 1.** Conceptual scheme of experiments.

### *2.2 Boundary conditions for Simulation*

Finite Element Method was carried out using tetrahedral (deformable) mesh with volumetric elements for the billet and triangular (rigid) surface elements for the dies, as illustrated in Figure 2. The average mesh size was enough refinement for high convergence in the calculations. Table 2 shows the boundary conditions used for modelling, including friction and thermal parameters. The forming velocity of the hydraulic press was calculated from displacement data acquired during forming by an LVDT (Linear Variable Displacement Transducer) coupled to the upper die and with the end in contact with the lower (stationary) die. Regarding the friction between the systems, the best fitting condition of no lubrication was chosen from the software database.

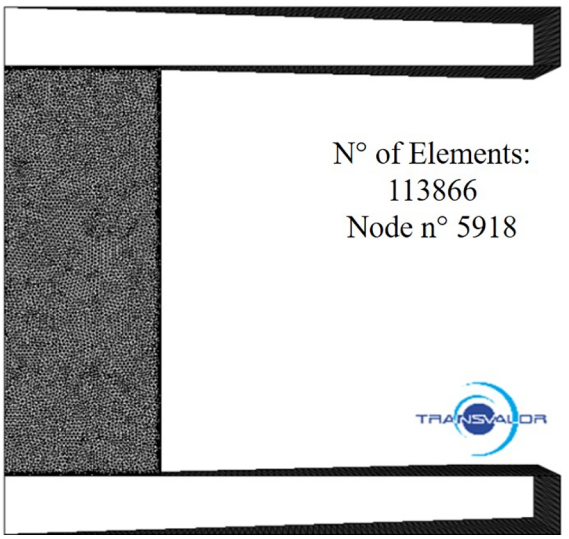


**Figure 2.** Modelling proposed.

**Table 2.** Boundary conditions used in the numerical computational simulation from the data collected in experiments.

| Parameters | Value |
|---|---|
| Initial steel temperature (°C) | 1180 |
| Environment temperature (°C) | 50 |
| Dies temperature (°C) | 190 Upper |
| Tool velocity (mm/s) | /250 Lower |
| Heat transfer coefficient with pressure (dies) (W/m$^2$.K) | 5 |
| Heat transfer ambient media (W/m$^2$.K) | 500 |
| Friction coefficient (Coulomb) | 10 |
| $(\overline{m}\ and\ \mu)$ | 0.8 and 0.4 |

### *2.3 Recrystallization modelling*

The recrystallization kinetics and austenitic grain growth were based on the global JMAK model. The output results consisted of the percentage value of the recrystallized fraction, as demonstrated in Equation (1).

This model is embedded into the commercial FEM metal forming software FORGE® software and can be seen in Table 3, where all the constants necessary to predict the behaviour in the recrystallization of DIN 20MnCr5 steel are presented [14]. Figure 3 shows a conceptual flowchart of the methodology used to perform the study and a comparison of the expected experimental results.

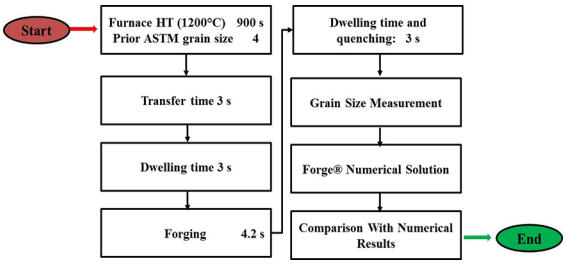


**Figure 3.** Conceptual flowchart used to compare experimental results and computational simulation.

In Table 3, critical strain ($\varphi_c$) is the minimum strain required for the dynamic recrystallization. The Zener – Hollomon parameter ($Z$) is a function of the strain rate as well as the material activation energy ($Q_{DRX}$) associated with recrystallization occurrence. This parameter is important because it establishes relationships between grain size and strain rate in the steel. The other kinetic parameters are related to recrystallization of DIN 20MnCr5 steel [14]. The $t_{0.5}$ is the time for $M_{DRX}$ equal to 0.5. The $d_0$ represents the initial grain growth and $d_{gg}$ the final grain growth for full recrystallization.

## 3. Results and Discussion

Figure 4 illustrates the temperature fields in the samples after forming for two different height reductions, 40 and 60%. A considerable decrease of temperature is seen in the upper and lower surfaces, which are in contact with the dies due to thermal exchange.

Figure 5 (a) and (b) show the effective strain and strain rate, respectively. An ample variation of the plastic strain field was observed from the centre of the workpiece, as well as the barrelling of the samples due to the frictional forces in the sample/die interfaces. The average strain rate increases in the sample corner regions due to the high friction. The sample/die contact increases the heat transfer in the interface, leading to lower temperatures for samples faces than in the middle.

Figure 6 (a) and (b) show, respectively, the Von Mises stress distribution and the fibering zone of the material as affected by shear stresses. After 60% of height reduction, higher local stresses are seen in the billet corners, which leads to an increase of strain rate and a decrease of the effective stress in the middle. The shear stress component increases gradually from the sample centre to the corner.

**Table 3.** Equations to describe the microstructure evolution.

| Parameters | Equation |
|---|---|
| **Recrystallization** | |
| Critical Strain | $\varphi_c = 3.92 \cdot 10^{-4} d_0^{0.5} \cdot Z^{0.15}$ |
| **Kinect parameters** | |
| Zener-Hollomonw | $Z = \dot{\varphi} \cdot e\left(\frac{310244}{RT}\right)$ |
| Dynamic recrystallization fraction, $D_{RX}$ | $X_{\mathrm{DRX}} = 1 - e^{\left(-0.693147 \cdot \left(\frac{\varphi - \varphi_c}{\varphi_{0.5} - \varphi c}\right)^2\right)}$ |
| 50% recrystallization, $D_{RX}$ | $\bar{\varphi}_{0.5} = 1.14 \cdot 10^{-3} \cdot d_0^{0.28} \cdot \dot{\varphi}^{0.05} \cdot Z \cdot e\left(\frac{53379}{RT}\right)$ |
| Static recrystallization fraction, $S_{RX}$ | $X_{SRX} = 1 - e^{\left(-0.693147 \cdot \left(\frac{t}{t_{0.5}}\right)\right.}$ |
| Metadynamic recrystallization fraction, $M_{DRX}$ | $X_{MDRX} = 1 - e^{\left(-0.693147 \cdot \left(\frac{t}{t_{0.5}}\right)\right)}$ |
| Time for 50% $M_{DRX}$, $t_{0.5}$ | $t_{0.5} = 1.06 \cdot 10 - {}^{5} \cdot Z^{-0.6} \cdot e\left(\frac{300000}{RT}\right)$ |
| **Grain Coarsening** | |
| For $D_{DRX}$ | $D_{DRX} = 2.26 \cdot 10^4 \cdot Z^{0,5}$ |
| For $S_{RX}$ | $D_{SRX} = 0.5 \cdot \bar{\varphi}^{-1} \cdot d_0^{0.67}$ |
| For $M_{DRX}$ | $M_{DRX} = 1,8 \cdot 10^4 \cdot Z^{0,5}$ |
| Diameter for a full $M_{DRX}$ | $t_{0.5} = 1800 \cdot Z^{-0,15}$ |
| Grain growth | $d_{gg}^{4,74} - d_0^{4,74} = 1,41 \cdot 10^{23} \cdot e^{\left(\frac{-433500}{RT}\right)} \cdot t$ |

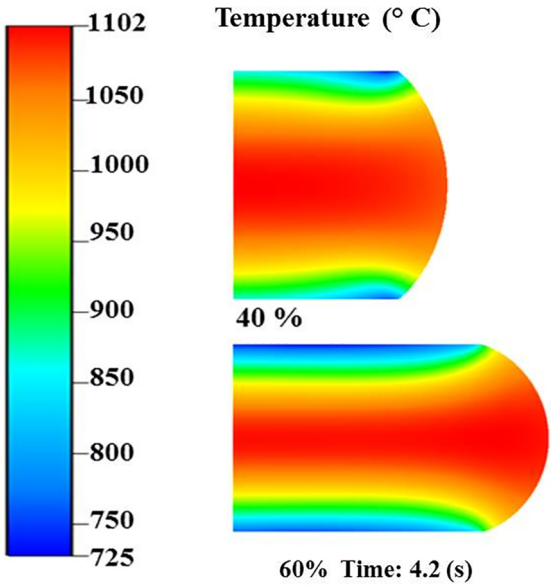


**Figure 4.** Numerical results of temperature fields after 40% and 60% height reduction.

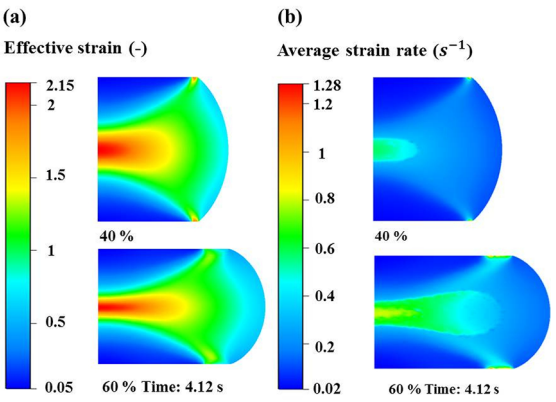


**Figure 5.** Numerical results of (a) Effective strain, (b) Average Strain rate.

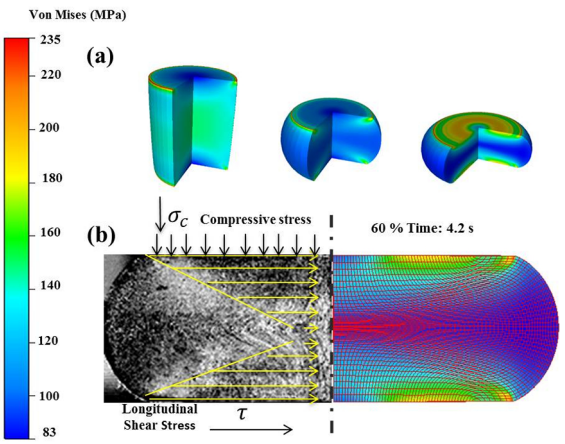


**Figure 6.** (a) Von Mises stress field, (b) Fibering and effect of stress triaxiality.

It is clear that the time evolution an distribution of stresses in the workpiece interact with strain rate and temperature, thus affecting recrystalization kinetics and finally the resulting austenitic grain size. Therefore, the temperature variation and the strain rate in the corners of the workpiece should be considered. This is an important issue to obtain a better agreement between the experimental process and simulation. Taking into account these considerations, forging parameters can be improved with the aid of FEM simulation.

Figure 7 (a) shows the dynamic recrystallization behaviour at 40% and 60% height reduction. In the centre of the sample with 60% reduction, a smaller recrystallized fraction is seen compared to other regions. According to Luton and Sellars[15], the reason for this could be that at lower strain rates and higher temperatures, distinct recrystallization cycles at a higher plastic strain are provoked. Furthermore, it could be associated with the shear stress gradient seen in the fibering zones (Figure 6 (b)). The evolution of parameter ($Z$), which depends on the strain rate, is presented in Figure 7 (b). There was a considerable increase in the Zener parameter, precisely in the corners of the workpiece, showing the proportionality of the shear stress and the increase of the strain rate. Sakai and Jonas [16] have already established relationships between the initial grain size and the parameter ($Z$), demonstrating that at higher strain rates, smaller nucleated grain sizes are reached. When the strain rate increases, hardening is increased, this consequently decreases the effect of dynamic recrystallization and recovery. Thus, the accumulated energy due to the increase of the dislocation density after the forging unloads provided the necessary driving force for the metadynamic recrystallization[17]. Different values of ($Z$) were found during the plastic deformation, which resulted in substantial grain size variations in the sample at the end of the process.

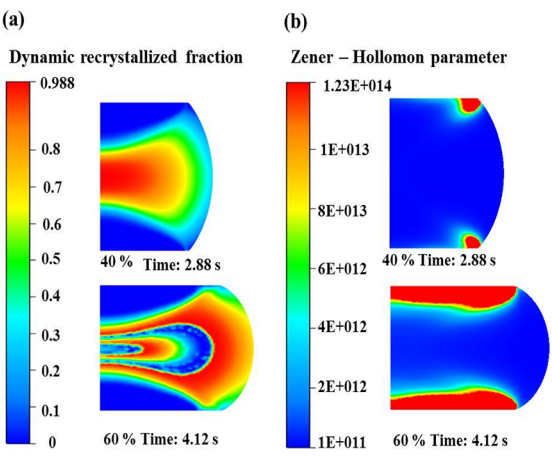


**Figure 7.** Numerical results of (a) Dynamically recrystallized fraction (XDRX), (b) Zener-Hollomon parameter.

In laboratory experiments with constant temperature, it is possible to correlate the amount of stored energy with the dislocation density to grain refining [18]. However, in an industrial environment using low-speed hydraulic presses, one must take into account the temperature distribution in the component, and how this also affects the strain rate and nucleation of new grains. In this way, heterogeneous strain distribution occurs in the workpiece, not only by triaxiality, which directly affects the austenitic grain size, as well as by different strain rates and temperature.

Figure 8 (a) displays the simulations results of austenitic grain size after 60% height reduction, at the final time of forging, while Figure 8 (b) shows the results after simulated water quenching. It is possible to observe that there is a significant increase in the grains after forging ending (unload) and 35 seconds after the water quenching process. The differences in grain size are due to the mechanisms of meta-dynamic recrystallization included in the FEM calculation.

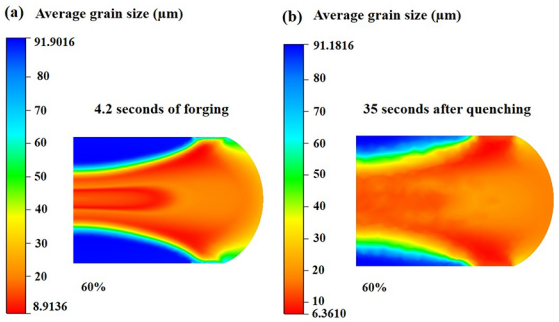


**Figure 8.** Numerical results of (a) Average grain size in the forging instant, (b) Average grain size after quenching.

Figure 9 (a) illustrates the calculated meta-dynamic and static recrystallization in the final stage. The temperature field at steady-state (after 35 seconds in water) resulted in a higher fraction of metadynamic recrystallized grains in the regions with lower strain, strain rate and temperatures.

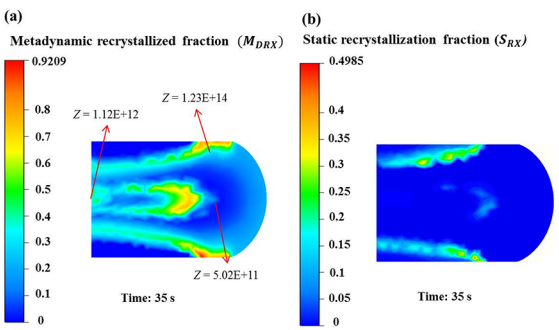


**Figure 9.** (a) Metadyninamic recrystallized fraction (MDRX), (b) Static ecrystallized fraction (SRX).

According to Hodgson [19], metadynamic recrystallization depends on the strain rate, being little influenced by temperature and alloying elements. However, the Zener parameter, which means the temperature corrected strain rate [16], was sensitive to forging temperature. Therefore, the temperature gradients must be taken into account during forming, for example, in the corners of the workpiece, where the ($Z$) value is larger and more refined grains were seen.

Figure 10 presents the results obtained from the experimental austenitic grain size in four different selected region (R1, R2, R3 and R4). The analysis of the microstructure shows an apparent variation of grain size, as predicted by numerical simulation, however different grain morphologies could be seen which represent different recrystallization mechanisms. Therefore, the temperature and strain rate variation corrected by $Z$ parameter should be considered in this case. In R1, there was no dynamic recrystallization (, therefore sheared and polygonal grain characteristics which could represent a static recrystallized fraction mechanism. Figure 9 (b) shows the calculated results for the same region R1. In the region R2 a metadynamic recrystallization, as well as a geometric coalescence of the grains, was observed. This is attributed to the more significant thermodynamic potential at this point. It was also observed in the experimental analysis that in the region R3 higher grain refining was found (20 μm), on the other hand for region R4 larger grain sizes (30 μm) were measured when compared to R2 and R3. Those results confirm the difference of the $Z$ parameter in both cases is related to the temperature variation, being lower in the middle of the workpiece.

Numerical simulated stress-strain curves for the forging process are shown in Figure 11(a), which presents several oscillations which are typical for dynamic recrystalization. The decrease in stress after each plateau may be attributed to the new $X_{DRX}$ cycle [20]. Figure 11 (b) shows the recrystallized fractions at each chosen region and the flow curve's response. It seems clear that an evident dynamic recrystallization cycle has occurred in R2 and R4. The reason for that is because there was both high temperature and considerable plastic strain, where new nucleated grains appear in the zone before full recrystallization ($X_{DRX} > 0.95$). Therefore, the degree of plastic strain coupled with the strain rate and temperature individually influenced the cycles of dynamic recrystallization showing the time required to reach the steady-state during the deformation process, as a function of $X_{DRX}$. The $X_{DRX}$ cycles in R2 is higher than R4 showing that the reduction of recrystallization rate decreases proportionally with the temperature, and can be confirmed in the R3 which presented the unfull recrystallization ( XDRX < 0.95).

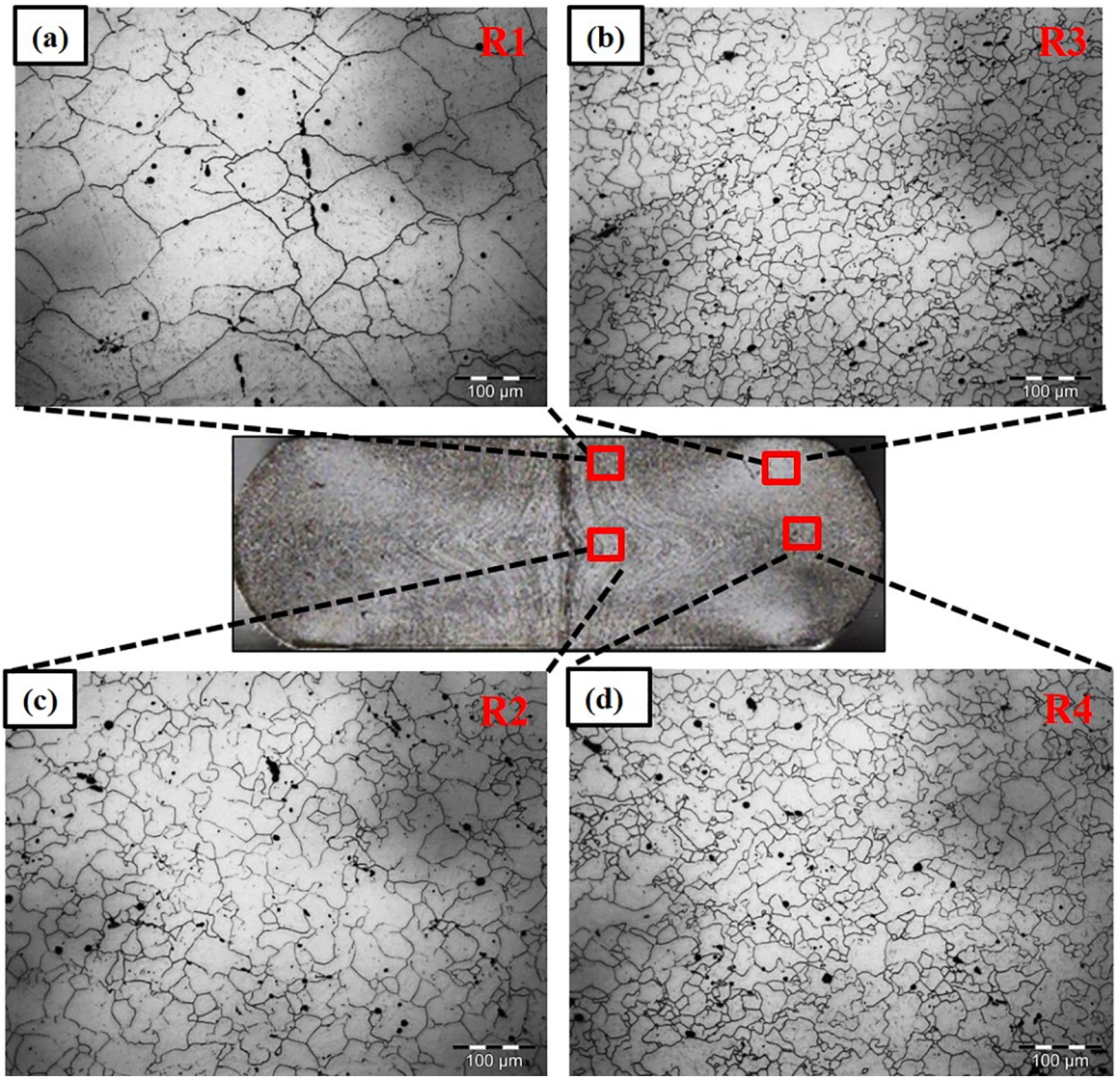


**Figure 10.** Experimental macrography and austenitic grain size results for forged and water quenched samples. Picral etching with 3vol. % Picric Acid in destined water.

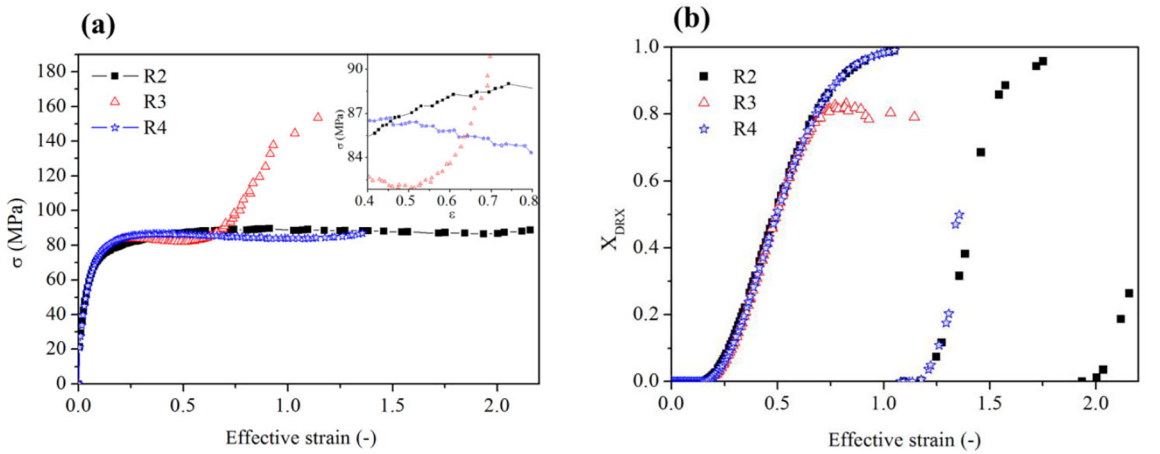


**Figure 11.** Numerical results of (a) Flow curves generated in different regions of the workpiece, (b) XDRX cycles response.

Figure 12 compares measured and simulated grain sizes at four selected regions after the quenching process. The general behaviour and the dependencies with processing parameters were well described by simulation, however differences in the absolute values are seen. Possibly a significant factor influencing the simulation results is the heat transfer model for the water quenching, which shows the importance of controlling thermomechanical history. Besides that, considering a large number of possible impressions in the input data, as flow curves for different temperatures and strain rates, friction coefficient, heat transfer coefficients, among others contribute to the observed differences.

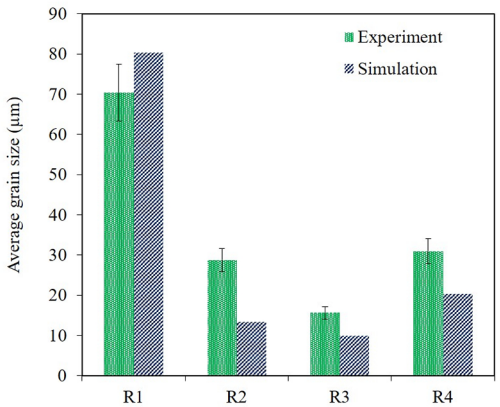


**Figure 12.** Average grain size comparison between experimental results and calculated.

## 4. Conclusions

This article showed the applicability of a model coupling the semi-empirical JMAK and a visco-elastoplastic model in numerical simulation of hot forging a 20MnCr5 steel followed by water quenching aiming at austenitic grain size prediction.

The results showed a good agreement between experimentally measured and simulated PAGS after hot forging and water quenching. Different distributions in austenitic grain size and recrystallized fractions were found in the forged part due to different strain-rate a temperature field, however, as demonstrated in this article the interaction of strain-rate and temperature plays an important role. The implemented models were able to detect those effects by showing the influences on the Zener-Hollomon parameter, which leads to PAGS non-homogenous distribution.

Finally, we can conclude that the numerical simulation using the already mentioned models is able to make a reasonable prediction of PAGS; however, there is still the need to improve boundary conditions with a precise determination of flow curves dependence on strain-rate and temperature.

## 5. Acknowledgement

The authors thank the Brazilian agency CAPES (Project 1844/2017) and the German agency DFG (Project ZO140/21-1) for the financial support by means of the BRAGECRIM program (Brazilian German Cooperation Research in Manufacturing). Thiago Ivaniski also thanks CNPq (process number 167948/2017-2) for scholarship support.

## 6. References

1. Jorge Junior AM, Balancin O. Prediction of steel flow stresses under hot working conditions". *Materials Research*. 2005;8(3):309-315.

2. Hanamura T, Torizuka S, Tamura S, Enokida S, Takechi H. Effect of Austenite Grain Size on Transformation Behavior, Microstructure and Mechanical Properties of 0.1C–5Mn Martensitic Steel. *ISIJ International*. 2013;53(12):2218-2225.

3. Sellars CM, Whiteman J A. Recrystallization and grain growth in hot rolling. *Metal Science*. 1978;13(3-4):187-194.

4. Jorge Junior AM, Regone W, Balancin O. Effect of competing hardening and softening mechanisms on the flow stress curve modelling of ultra-low carbon steel at high temperatures. *Journal of Materials Processing Technology*. 2003;142(2):415-421.

5. Lan LY, Qiu CL, Zhao DW, Gao XH, Du LX. Dynamic and Static Recrystallization Behavior of Low Carbon High Niobium Microalloyed Steel. *Journal of Iron and Steel Research International*. 2011;18(1):55-60.

6. Mirzadeh H, Najafizadeh A. Prediction of the critical conditions for initiation of dynamic recrystallization. *Materials and Design*. 2009;31(3):1174-179.

7. Hallberg H. Approaches to Modeling of Recrystallization. *Metals (Basel)* [Internet]. 2011; 1(1):16-48. Available from: http://www.mdpi.com/2075-4701/1/1/16/

8. Bylya O, Reshetov A, Stefani N, Rosochowska M, Blacwell P. Applicability of JMAK-type model for predicting microstructural evolution in nickel-based superalloys. *Procedia Engineering*. 2017;207:1105-1110.

9. Stefani N, Bylya O, Reshetov A, Blackwell P. On the applicability of JMAK-type models in predicting IN718 microstructural evolution. *Computer Methods in Materials Science*. 2017;17(1):59-68.

10. Bylya OI, Sarangi MK, Rohit N, Nayak A, Vasin RA, Blackwell PL. Simulation of the material softening during hot metal forming. *Archives of Metallurgy and Materials*. 2015;60(3A):1887-1893.

11. Moraes ALI, Balancin O. Numerical Simulation of Hot Closed Die Forging of a Low Carbon Steel Coupled with Microstructure Evolution 2. *Materials Research*. 2015;18(1):92-97.

12. Irani M, Joun M. Determination of JMAK dynamic recrystallization parameters through FEM optimization techniques. *Computational Materials Science*. 2018;142:178-184.

13. Irani M, Lim S, Joun M. Experimental and numerical study on the temperature sensitivity of the dynamic recrystallization activation energy and strain rate exponent in the JMAK model. *Journal of Materials Research and Technology*. 2019;8(2):1616-1627. DOI: https://doi.org/10.1016/j.jmrt.2018.11.007

14. FORGE®. FORGE NxT V 2.1. System Documentation,Transvalor, Sophia Antilopis, Cedex; 2018.

15. Luton MJ, Sellars CM. Dynamic recrystallization in nickel and nickel-iron alloys during high-temperature deformation. *Acta Metallurgica*. 1969;17(8):1033-1043.

16. Sakai T, Jonas JJ. Overview no. 35 Dynamic recrystallization: mechanical and microstructural considerations. *Acta Metallurgica*. 1984;32(2):189-209.

17. Shen WF, Zhang C, Zhang LW, Xia YN, Xu YF, Shi XH. Metadynamic recrystallization of Nb-V micro-alloyed steel during hot deformation. *Journal of Materials Research*. 2017;32(3):656-65.

18. Lin YC, Chen MS, Zhong J. Numerical simulation for stress/strain distribution and microstructural evolution in 42CrMo steel during hot upsetting process. *Computational Materials Science*. 2008;43(4):1117-1122.

19. Hodgson PD, Gibbs RK. A Mathematical Hot Rolled C-Mn Model to Predict and Microalloyed the Mechanical Properties of Steels. *ISIJ International*. 1992;32(12):1329-338.

20. Mirzadeh H, Najafizadeh A. Hot Deformation and Dynamic Recrystallization of 17-4 PH Stainless Steel. *ISIJ International*. 2013;53(4):680-689.